

## ARTICLE

DOI: 10.1038/s42004-018-0073-4

OPEN

# Light actuated swarming and breathing-like motion of graphene oxide colloidal particles

Hong Qin<sup>1</sup>, Xiaoran Wu<sup>1</sup>, Xiang Xue<sup>1</sup> & Hewen Liu <sup>1</sup>

Synthetic microparticles that can be propelled under light stimulus and generate collective behaviors via interaction among these particles may lead to applications in numerous fields. Here we show that aqueous graphene oxide (GO) particles can move autonomously to a light source. These self-propelled multilayer GO particles swarm but periodically “stop to take a breath” under continuous light stimulus. UV light causes a movement velocity of approximately  $25 \mu\text{m s}^{-1}$  and oscillating frequency of approximately two times per minute for multilayer GO particles. Light with a wavelength longer than green light causes neither locomotion nor oscillation. Only multilayer GO particles exhibit the oscillating behavior. This unusual oscillating mode suggests that multilayer GO particles may undergo non-equilibrium dynamic processes in their light-actuated collective motion.

<sup>1</sup>CAS Key Laboratory of Soft Matter Chemistry, Department of Polymer Science and Engineering, University of Science and Technology of China, 96 Jinzhai Road, Hefei, Anhui 230026, P. R. China. Correspondence and requests for materials should be addressed to H.L. (email: [lhewen@ustc.edu.cn](mailto:lhewen@ustc.edu.cn))

Self-propelled colloidal particles have continuously attracted broad interests in various fields including materials sciences, surface/interface sciences, biophysics and fluid mechanics<sup>1–5</sup>, not only because that the self-propelled colloid particles have potential applications in small smart devices, self-adaptive catalyst systems, etc<sup>6–10</sup>, but also because that their collective motion can generate order far from equilibrium<sup>11–13</sup>. The photo actuated self-driven phototactic particles are particularly interesting due to the “clean” propulsion way avoiding additional chemicals and remote controllable behaviors, etc<sup>14</sup>. The collective motion of schooling active matters often generates either non-equilibrium ordered patterns or synchronized motility to generate fluid flows or to effectively function, for example, schools of fish, flocks of birds, flagella, and even some cells<sup>13,15,16</sup>. Collective dynamic motion is still a highly non-trivial topic. Some theoretical dynamic models have been established for investigating the emergence of order far from equilibrium<sup>11,12,17,18</sup>. Nevertheless, synthetic colloidal particles that are capable of synchronized motility are still rarely observed thus far to our knowledge.

Graphene oxide (GO) and graphene are two-dimensional (2D) materials with unique electronic properties and have been investigated intensely in recent years<sup>19,20</sup>. GO and graphene have also been used in preparing self-propelled microparticles, exploiting the confined space of GO to release gas for propulsion<sup>21,22</sup>, or wrapping silica microparticles with graphene for preparing surface conductive Janus microparticles capable of self-electrophoresis<sup>23</sup>. Though GO is characterized by its impressive surface area and special surface/interface properties, however, the surface phoretic effects of GO colloidal particles (including electrophoretic, nonionic/ionic diffusiophoretic, or thermophoretic effects<sup>4</sup>) are not investigated in the literature yet.

Here we show that GO colloidal particles undergo self-propelled movement under light stimulus. We find that multi-layer GO colloidal particles can autonomously swarm and periodically “stop to take a breath” synchronously under continuous light stimulus.

## Results

**Light-induced swarming and oscillating.** In order to guarantee the objectivity and generality of results, we purchased two kinds of GO reagents including GO powder and GO flake (containing ~99% single layer GO as declared in the product datasheet) (XFNano, Inc., Nanjing, China) to prepare colloidal GO particles for the research of this work. Two kinds of colloidal particles GO were obtained by dissolving these GO reagents in ultrapure water (18.3 M $\Omega$  cm) under ultrasonication for 3 h and successive natural sedimentation overnight, i.e., the dispersed GO particles, and the precipitated GO particles at bottom. Both colloidal particles GO were obtained from the GO powder reagent. When we used the GO flake reagent, only the dispersed GO particles were obtained in this way. It was hard to find differences between the dispersed and the precipitated GO particles either under a scanning electron microscope or with Raman spectroscopic analysis. However, the dispersed and the precipitated GO particles showed different mean thicknesses measured with atomic force microscopy (AFM) by averaging over images of randomly chosen ~100 platelets, according to the method reported in the literature (Fig. 1)<sup>24</sup>. For the dispersed GO particles, the minimum sheet thickness is ~1 nm and the peak of the thickness distribution appears at ~3 nm with the mean of ~13 nm (e in Fig. 1). The dispersed GO particles were loose aggregations of single-layer GO or its folding structures. In contrast, the precipitated GO particles have a mean thickness of ~79 nm (d in Fig. 1), and the peak of the thickness distribution appears at ~20 nm, much thicker than dissolved GO. The precipitated GO

particles could be further exfoliated when subjected to ultrasonication in additional 6 h, and the mean thickness becomes ~20 nm (c in Fig. 1) with nearly the same distribution as that of dispersed GO particles. We carried out the X-ray diffraction (XRD) analysis on the dry samples of the dispersed and the precipitated GO particles (Fig. 1). In the XRD patterns, the strong and sharp (002) peak at  $2\theta = 8.99^\circ$  and  $10.37^\circ$  corresponds to an interlayer distance of 9.83 Å and 8.52 Å for the dispersed and the precipitated GO particles, respectively. No obvious graphite diffraction peaks are found in the XRD of either the dispersed or the precipitated GO particles. We also measured the longest dimension (the lateral size) of ~100 objects with AFM with the data presented in Fig. 1 as a histogram. Though the AFM length is possibly overestimated owing to broadening effects from the interactions between cantilever and substrate/sample<sup>25</sup>, however, the data are accurate enough for comparison in this work. The precipitated GO has a bit bigger average lateral size than the dispersed GO. Its average sizes do not change greatly after thoroughly ultrasonication (Fig. 1). Overall, AFM and XRD analysis proved that the precipitated GO particles were mainly compact stacks of GO sheets. To distinguish different GO particles, we call the precipitated GO particles as stacked GO particles below. Finally, we adjusted the weight contents of the dispersed or the stacked GO particles to particular concentrations for successive investigation.

The dispersed GO particles (0.5 mg mL<sup>-1</sup> if not stated otherwise) swarmed toward the incident UV beam (wavelength of 330–385 nm) focused through a microscope lens emitting from the built-in illumination source of an inverted fluorescence microscope (Supplementary Movie 1). The swarming is a kind of light-induced locomotion, because of the following experimental results:

The first, the movement was directed toward the center of light beam. And if we moved the sample stage against the UV beam, the swarming center moved with the center of UV beam. The motile particles finally aggregated at the bottom of the container, and only one aggregate was observed. The reasons may be twofold. The light-induced propulsion in GO particles was generated owing to the asymmetric light absorption in a light field not due to asymmetric particle shape. The asymmetric propulsion forces generated from surface photochemical/physical reactions are sensitive to the asymmetric light absorption, and thus are always directed towards the light source. Even a perfect spherical particle in a light field can be divided by asymmetric light absorption into two parts, dark side and bright side, as was pointed in our previous work<sup>14</sup>.

The second, the root-mean-square (RMS) phototaxis velocity was dependent on the incident light intensity, as is depicted in Fig. 2a. When the UV intensity increases from 89 mW cm<sup>-2</sup> to 192 mW cm<sup>-2</sup>, the RMS velocity of GO increases from 17  $\mu\text{m s}^{-1}$  to 25  $\mu\text{m s}^{-1}$ . GO particles do not swarm in UV light beam with intensity of 34 mW cm<sup>-2</sup> or weaker. The UV light with intensity of 192 mW cm<sup>-2</sup> was adopted for usual experiments.

The third, the locomotion was also photo-switchable. Repeated UV ON-OFF experimental results are illustrated in Fig. 2b. If the UV light was shuttered, the phototaxis of GO micromotor slowed down from ~25  $\mu\text{m s}^{-1}$  to 0  $\mu\text{m s}^{-1}$  in a couple of seconds. If the shutter of the UV light was open, the locomotion started again immediately.

The fourth, the velocity of the locomotion was related to the stimulus photo energy. By changing the filter cubes, we can change the incident photo energy. Four filter cubes we used in this work are WU (UV, 330–385 nm), WIBA (blue light, 460–495 nm), WIG (green light, 530–550 nm) and CY5 (orange red light, 590–650 nm). UV causes the fastest RMS velocity (~25  $\mu\text{m s}^{-1}$ ), followed by WIBA (~12  $\mu\text{m s}^{-1}$ ) and WIG (~7  $\mu\text{m s}^{-1}$ ) (Fig. 2c).

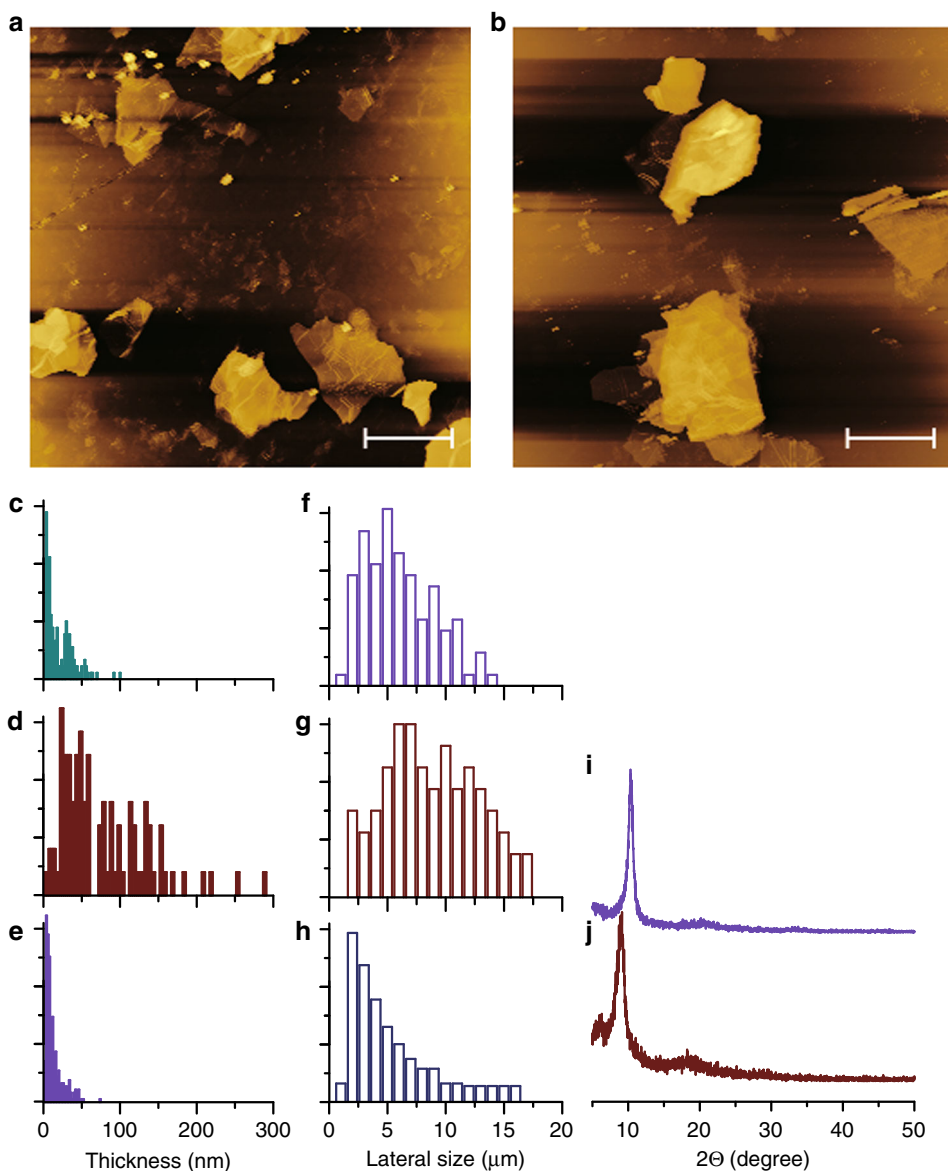


**Fig. 1** AFM and XRD analysis of the dispersed and the precipitated GO particles. AFM image of the dispersed **a** and the precipitated GO **b**. The bar in **a** and **b** is 10  $\mu\text{m}$ . Histogram of sheet thicknesses from AFM images of 140 sheets: **c** the precipitated GO after ultrasonication in additional 6 h, **d** the precipitated GO, **e** the dispersed GO. Histogram of lateral sizes from AFM images of  $\sim 100$  sheets: **f** the precipitated GO after further ultrasonication in additional 6 h, **g** the precipitated GO, **h** the dispersed GO. XRD patterns of the dispersed **j** and the precipitated GO particles (**i**)

The orange red light cannot generate enough thrust even at a high light density in this work. This indicated that the propulsion was likely generated from surface photochemical reactions, which rely on light exceeding a certain threshold energy. Along with the increasing UV exposure time, the locomotion velocity decreases (Fig. 2d). Overall, the locomotion of GO particles is light-induced phototaxis.

The stacked GO particle ( $0.1 \text{ mg mL}^{-1}$  if not stated otherwise) could also swarm like the dispersed GO particles. However, we found a special kinematical characteristic of the stacked GO particles after long time observation, i.e., the locomotion of the stacked GO particles was actually a directed swarming intermingled with short pauses under continuous light stimulus, as if these mobile GO particles could autonomously “stop to take a breath and go” (Supplementary Movies 2–5). To a certain motile particle at low Reynolds number where inertial effects can be ignored, pause means vanishing of net force gradients. To confirm the nonlinear oscillating behavior, we excluded the

possibility of doubt, for example, fluctuation of luminous intensity, recording software freezing, etc. We once placed fluorescent nanoparticles outside the container on the sample stage. The glow emanating from the fluorescent nanoparticles did not change during the pause of the moving GO particles under steady UV light (Supplementary Movie 2).

There was an induction period between the beginning of swarming and the onset of “breathing”, normally 5–30 minutes. The swarming with periodic pauses is a kind of oscillation, which originates in nonlinear systems that are far from equilibrium. The induction time is perhaps necessary for GO particles to reach an oscillatory state far from equilibrium, same as the time delay found in the chemical oscillations of an aqueous suspension of silver orthophosphate microparticles<sup>26</sup>.

The oscillatory characteristic of the stacked GO particles was clearly demonstrated in the deposits of the precipitated GO particle at the bottom. As the light-driven phototaxis lasted a while, GO particles aggregated and deposited on the bottom.

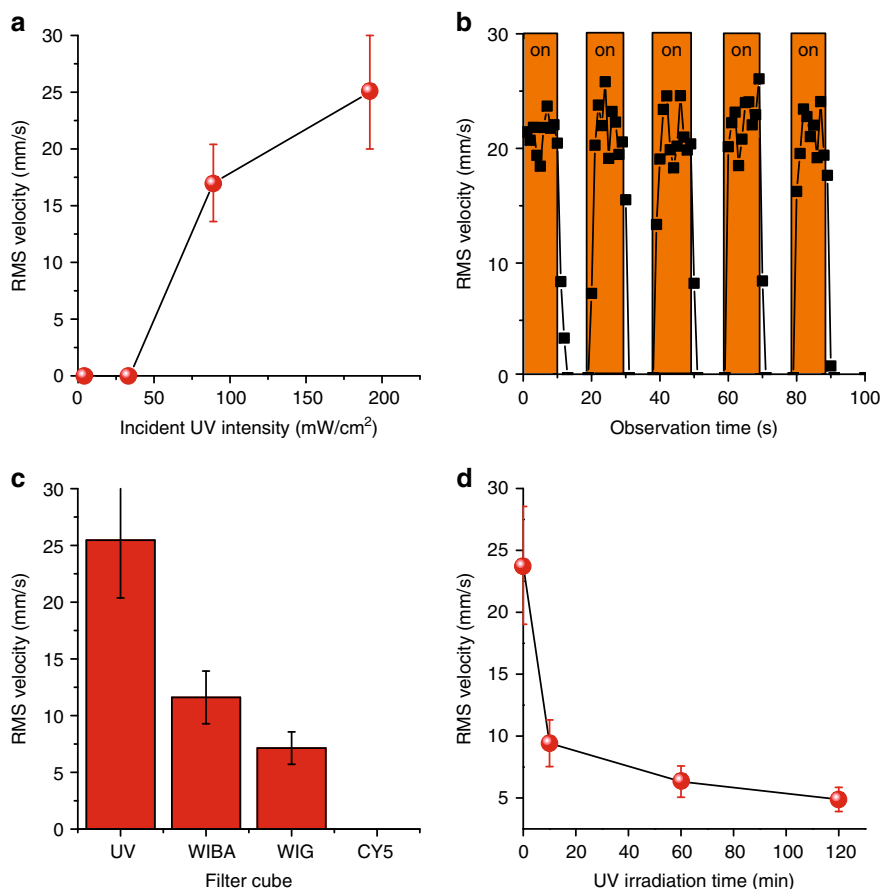


**Fig. 2** Some factors affecting the light-induced phototaxis of the dissolved GO particles. **a** UV intensity. **b** Light (UV) switchability. **c** Light energy. **d** UV irradiation time. Calculation of RMS velocity is defined in the Methods; briefly, RMS velocity is calculated by  $\langle \Delta L^2 \rangle^{1/2} \Delta t^{-1}$ . Error bars are calculated as half of the standard deviation of  $\langle \Delta L^2 \rangle$

During the short pause period, the stacked GO particle lost the propulsion force, and the stress to press the deposits shrinking relieved, and then the deposits began to expand slightly. The automatic and periodic contraction and expansion under continuous light stimulus looked like that the stacked GO particles were oscillating (Supplementary Movie 3). Fig. 3a depicted the periodic changes of the diameters of the deposits and the RMS velocity in a randomly selected period. As shown in Fig. 3a, during the pause (16–28 second), the GO particles look almost still with the RMS velocity of  $\sim 1 \mu\text{m s}^{-1}$ , and the diameter of the deposits expands from  $115 \mu\text{m}$  to  $122 \mu\text{m}$ . So, the pause stage is actually a very slow locomotion, which is clearly shown by video playback at a high speed, for example,  $8\times$  speed. After the pause, the RMS velocity of the GO particles rapidly increases from  $1 \mu\text{m s}^{-1}$  to  $15 \mu\text{m s}^{-1}$ , and the diameter of the aggregates decreases from  $122 \mu\text{m}$  to  $112 \mu\text{m}$ . The typical change in the diameter of the deposit is illustrated in Fig. 3d. If we moved the sample stage against the UV beam, the deposits moved with the center of UV beam while oscillation was not interrupted (Fig. 3e, and Supplementary Movie 4 in the supporting info). The recorded videos showed that the oscillatory kinematic behavior of the schooling particles seemed independent of the size and shape of the deposits (Supplementary Movie 4–6). The oscillation could occur at the “head” of migrating deposits with shifting light source according to the Supplementary Movie 4, and could also occur at the beginning of deposition with a small size of deposits (Supplementary Movie 5 and 6).

The average oscillating frequency of the oscillatory process is related to the stimulus light sources (Fig. 3b). For the same

sample, UV light causes the fastest frequency (about two times per minute), followed by blue and green light. Orange red light could not cause either locomotion or oscillation. The contents of GO affect the oscillation of the GO particles as well (Fig. 3c). Roughly, only when the contents of GO are in the range from  $0.05$  to  $\sim 0.10 \text{ mg mL}^{-1}$ , the stacked GO particles can oscillate under continuous light stimulus. The content range of GO suitable for swarming is broader. Only when the contents of GO are higher than  $5.0 \text{ mg mL}^{-1}$ , all the GO particles including the dispersed and the stacked GO particles cannot move at all, seemingly being damped by too many particles.

We found that the stacked multilayer structures are important for achieving the oscillation of GO particles under steady light stimulus because of the following facts. The first, the dispersed GO particles that are aggregates or loose stacks of single layer GO sheets can just swarm without pauses. The second, when the stacked GO particles were subjected to further ultrasonication in additional 6 h for thoroughly delamination, the obtained GO particles with the mean thickness close to that of the dissolved GO particles could not “breathe” any more. The diameters of GO particles after thoroughly ultrasonication did not change significantly. Thus, we think that it is the thickness difference not the diameter difference that caused the kinematical difference between the dispersed and the stacked GO particles. The third, if we used the fully soluble GO flake reagents containing 99% single layer GO, we could not observe the oscillation phenomena. However, we succeeded in preparing the stacked multilayer GO particles from GO flakes either by chemical cross-linking of the GO flakes with ethylene diamine

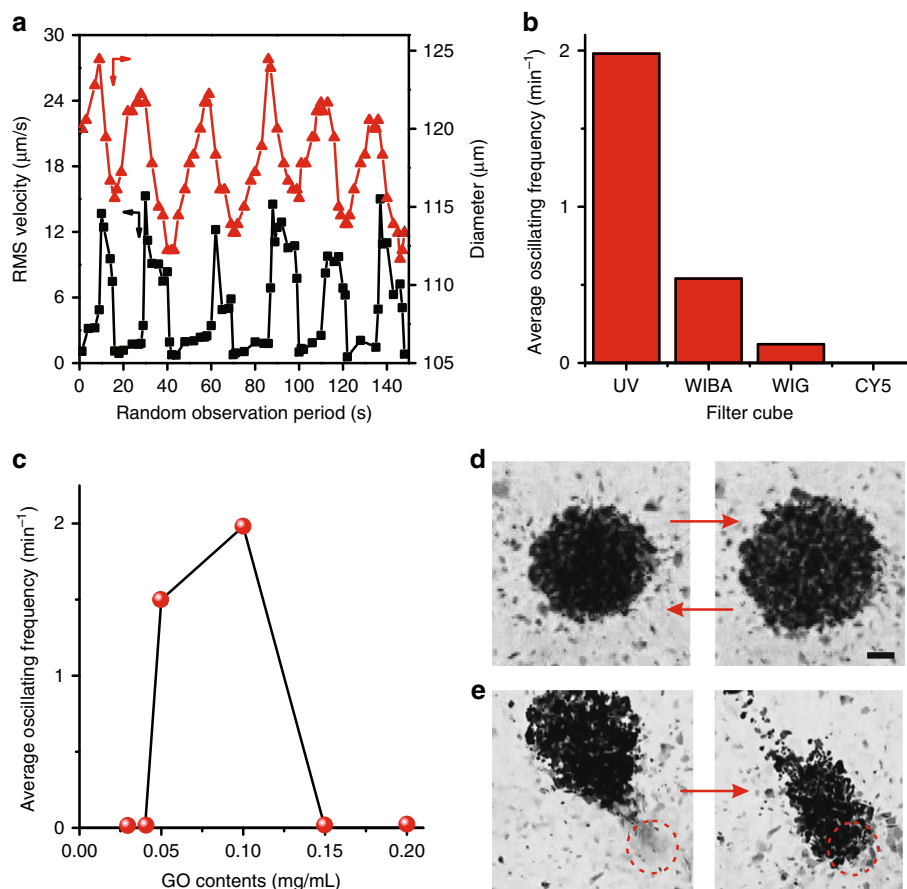


**Fig. 3** Oscillation of the deposits of the stacked GO particles. **a** Change of the deposit diameter and the phototaxis velocity. **b** Dependence of the oscillation frequency on light energy. **c** Oscillation frequency at different GO contents. **d** Images illustrating the reversible change in the size of deposits. **e** The deposits shifting with the center of the incident light beam (marked with a circle). The bar is 20  $\mu\text{m}$  for **d** and **e**

or by physical cross-linking of the GO flakes through partially reduction with dilute hydrazine. We supposed that ethylene diamine could fix the stacked multilayer structures of GO by linking the carboxylic or epoxide groups between layers. Dilute hydrazine solution can partially reduce GO to form hydrophobic reduced GO zones in a GO sheet by which the compact multilayer structures of GO can also be fixed. The multilayer structures of these fixed GO particles retained after rigorous ultrasonication, supported by the AFM analysis (Fig. 4). The mean thickness of the ethylene diamine fixed GO particles and the hydrazine fixed GO particles is 47 nm and 38 nm, respectively, whereas the mean thickness of the pristine dispersed GO particles is 18 nm (Fig. 4 d, e, and f). The two chemically fixed GO particles and the pristine GO flakes have almost the same distribution of lateral sizes with the mean of  $\sim 4 \mu\text{m}$  (Fig. 4 g, h, and i). The morphologies of the two fixed GO particles look the same as the dispersed GO particles under AFM (Fig. 4 a and b). XRD analysis on these GO particles shows the strong (002) peak at  $2\theta = 10.38^\circ$  in the ethylene diamine fixed GO particles and  $12.38^\circ$  in the hydrazine fixed GO particles correspondent to an interlayer distance of 8.52  $\text{\AA}$  and 7.14  $\text{\AA}$ , respectively (Fig. 4 o and n). Both fixed multilayer GO particles could oscillate during their motion processes (Supplementary Movie 6 of the hydrazine fixed GO particles and Supplementary Movie 7 of the ethylene diamine fixed GO particles). It was noticed that reduction degree of GO by hydrazine should be limited. Otherwise, the aqueous stability of the obtained colloidal particles was bad, and the surface phoretic effects for propulsion might be also affected.

We also used hexamethylene diamine instead of ethylene diamine to fix the multilayer structures of GO. However, we did not observe the oscillation phenomenon in the hexamethylene diamine fixed GO particles. We checked the morphology of hexamethylene diamine fixed GO particles with AFM, and found that the GO sheets were highly wrinkled (Fig. 4c). Because of the hydrophobicity, hexamethylene diamine adsorbed on GO caused the wrinkling of each single layer of GO and hindered the stacking of GO layers. The XRD analysis on the hexamethylene diamine fixed GO particles showed that the strong d002 peak at  $2\theta = 9.71^\circ$  correspondent to an interlayer distance of 9.10  $\text{\AA}$  (Fig. 4m), which is a bit bigger than that in the dissolved GO particles (8.39  $\text{\AA}$ ) or the ethylene diamine fixed GO particles (8.52  $\text{\AA}$ ). Folding instead of stacking of GO sheets may prevail in the hexamethylene diamine fixed GO particles. Overall, the stacked multilayer structure is important for the swarm-and-breathe behavior of GO particles.

**Self-propulsion mechanism.** Because of the carbonaceous nature of GO, we investigated the possible contribution to the light-induced propulsion of GO particles from light generated thermal gradients, with graphite powder as control. Graphite is regarded to be able to transfer the absorbed light energy into heat and be inert to UV irradiation especially to the weak UV source equipped in an optical microscope in this work. The tiny graphite particles underwent random thermal motion under UV induction, but bigger graphite particles seemed still (Supplementary Movie 8). However, it is found on a longer time scale that all the

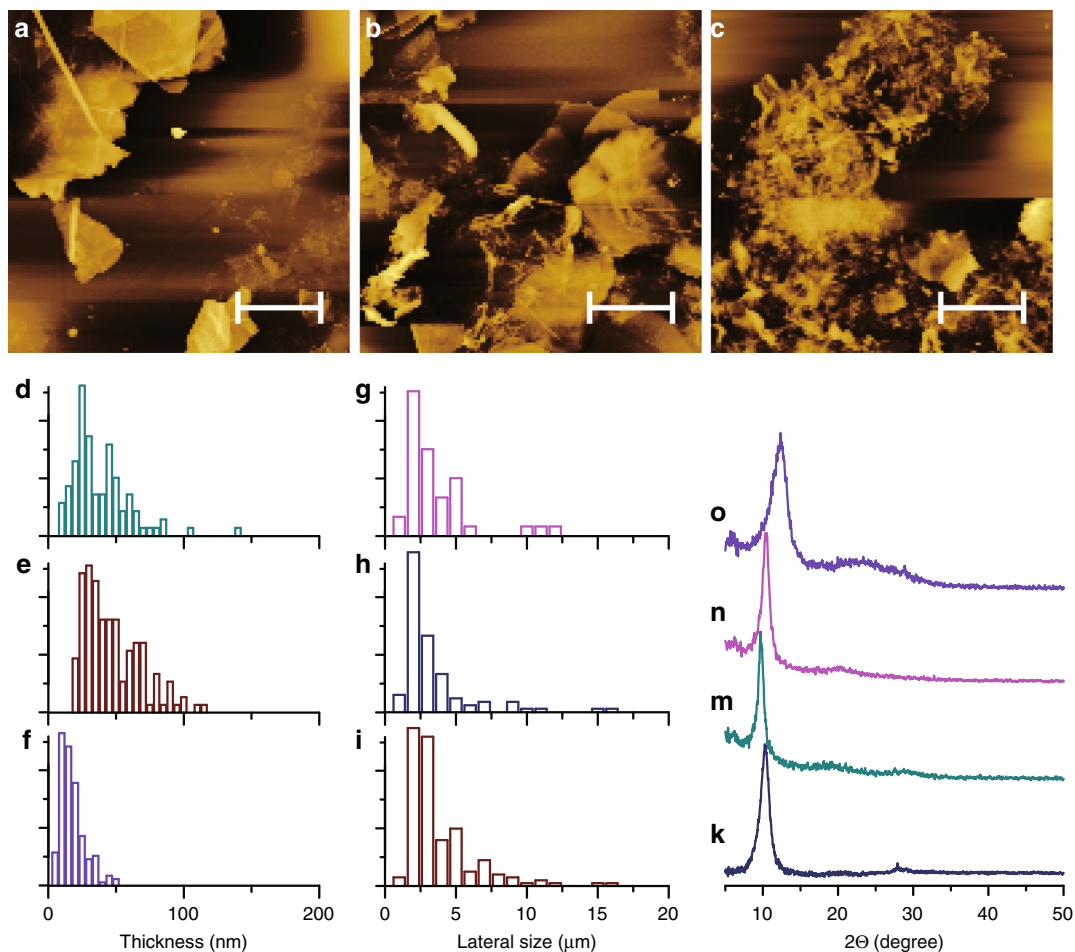


**Fig. 4** AFM and XRD analysis of the chemically fixed GO particles. AFM images of **a** the ethylene diamine fixed GO particles, **b** the hydrazine fixed GO particles and **c** the hexamethylene diamine fixed GO particles. The bar in **a**, **b**, and **c** is 5  $\mu\text{m}$ . Histogram of sheet thicknesses from AFM images of 140 sheets: **d** the hydrazine fixed GO particles, **e** the ethylene diamine fixed GO particles and **f** the pristine GO flakes. Histogram of lateral sizes from AFM images of 140 sheets: **g** the hydrazine fixed GO particles, **h** the ethylene diamine fixed GO particles and **i** the pristine GO flakes. XRD patterns of **k** the pristine GO flakes, **m** the hexamethylene diamine fixed GO particles, **n** the ethylene diamine fixed GO particles, and **o** the hydrazine fixed GO particles

graphite particles swarmed to the center of light beam actually with a very slow velocity of  $\sim 0.07 \mu\text{m s}^{-1}$ . Thus thermophoresis is not the principal cause of the light-induced swarming of GO particles.

We further investigated the mechanism of the self-propulsion of GO particles and found that the phototaxis of GO particles is self-electrophoresis according to the following experimental facts. The principle of self-electrophoresis has been described in the literature<sup>2,27,28</sup>. A self-electrophoretic colloidal particle is propelled by its self-generated electric field where the ions in the double layer migrate against the particle surface, and the particle moves against the fluid.

First, we carried out a simple experiment to verify the photo-generated electric field in the GO dispersions. The colloidal GO dispersion was placed in a silica tube (inner diameter 4 mm) with two platinum electrodes at both ends (1 cm apart). One half of the tube was shielded with black tape, and another half was exposed to UV light (Fig. 5a, b). We measure the voltage between the dark side and the bright side. A positive voltage is immediately generated from the bright side to the dark side when UV is turned on, and the voltage increases with exposure time at first and then reaches a stable value in  $\sim 2$  minutes (Fig. 5c). The positive voltage reveals that the electric field radiates from the center of the light beam to outside.

Second, the zeta potentials of GO particles are  $\sim -30$  mV, and increase with longer UV irradiation time, indicating that more cations are produced and adsorbed on the surface of GO particles (Fig. 5(d)). The change of zeta potentials vs. time can account for the results depicted in Fig. 2d. Thus, the motion direction of negative GO particle is toward the center of light beam.

Third an electrical connection in GO particles is necessary to drive the motion of GO particles through an electrokinetic mechanism. The UV-induced current of GO under the conditions of this work was measured according to the literature method<sup>29</sup>, as illustrated in Fig. 5e. The current generated from GO under UV is photo-switchable and becomes stronger as the relative intensity of UV light increases.

Fourth, UV exposure also causes the change in both the pH value and ionic conductivity of the GO particle dispersions, as demonstrated in Fig. 5f. According to Fig. 5f, when UV light is turned on, the pH decreases, while the ionic conductivity increases. The aqueous GO particles will produce  $\text{H}^+$  under UV irradiation, causing the changes in pH and the ionic conductivity. The migration of GO particles starts in line with the onset of increase in conductivity of GO dispersions. The changes are somewhat reversible. If UV light is turned off, both the pH and the ionic conductivity recover, and locomotion of GO particles stops.

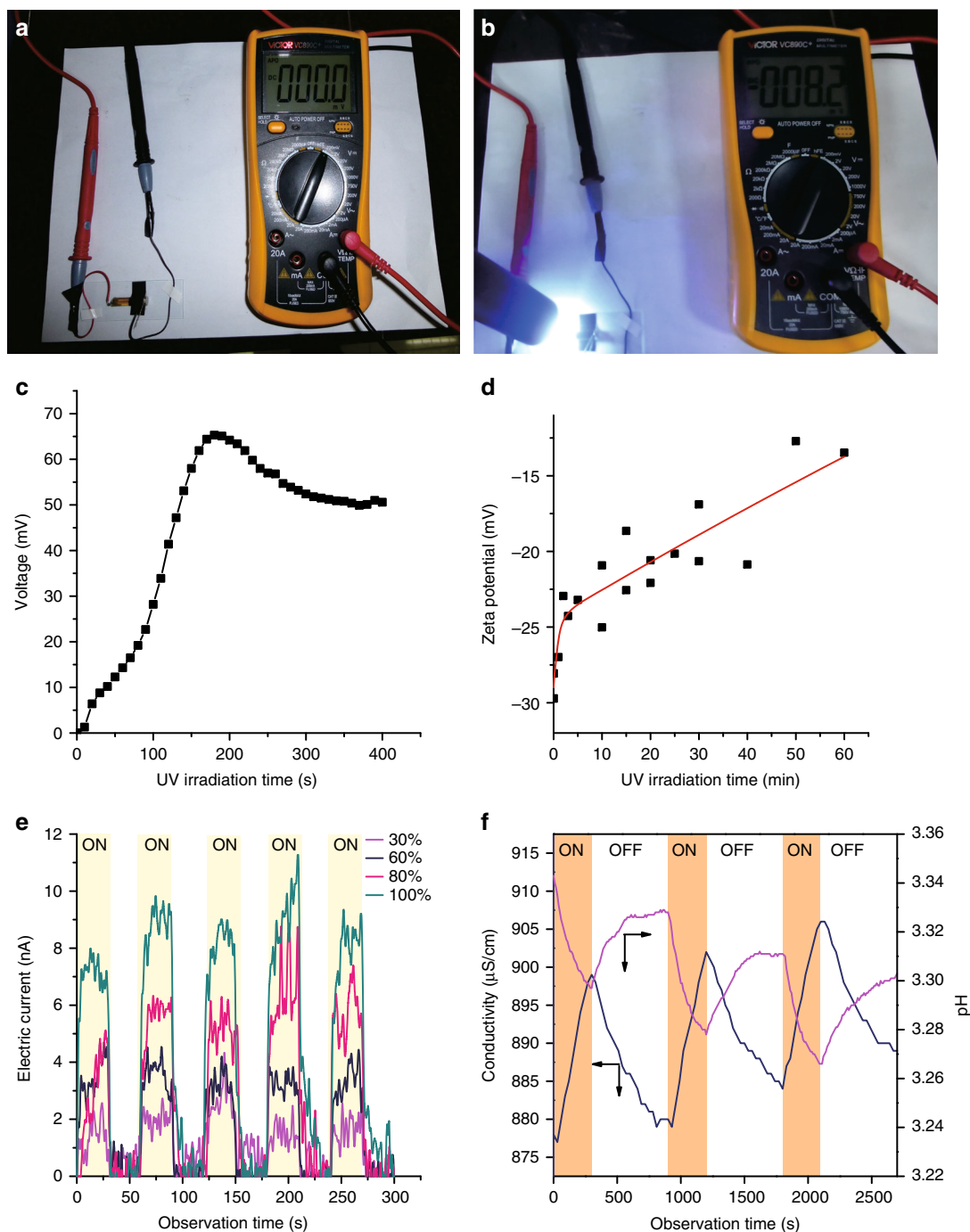


**Fig. 5** Photo-responsive electrical characteristics of colloidal GO particles. **a** and **b** are the photographs of the self-built devices for measuring the photo-generated electric field in the GO dispersions **a** before and **b** under light illumination, respectively. **c** The change of voltage with UV irradiation time. **d** The surface zeta potential of colloidal GO particles at different UV irradiation time. The red line is the trend line. **e** Switchable response of photo-generated current to ON-OFF UV exposure time and different relative intensities. **f** Switchable response of the ionic conductivity and pH value of the GO dispersions to ON-OFF UV exposure time

It appears that the propulsion of the motile GO particles is generated in the photoreactions of GO in water. The photoreactions of aqueous GO are very complicated, and many mechanisms have been suggested, including reduction by solvated electrons produced in UV photoionization of water, or photocatalyst reactions through the  $sp^2$ -semiconducting domains of GO<sup>30–32</sup>. It is noticed that there is a photoionization threshold (6.5 eV) for the generation of solvated electrons in water<sup>30</sup>. The structure of GO can be regarded as

semiconducting  $sp^2$  domains with domain size dependent band gap surrounded by insulating  $sp^3$  defects. Irradiation with light of energy exceeding their band gap causes electron jump to form excited electrons and holes responsible for the photoreactions of GO and water. The minimum energy for the electronic transition in GO is  $\sim 1.90$  eV<sup>32</sup>. Considering the fact that there is a light energy threshold for the self-propulsion or breathing of GO, it is reasonable to state that the photoreactions for generating the thrust start with the electron transition

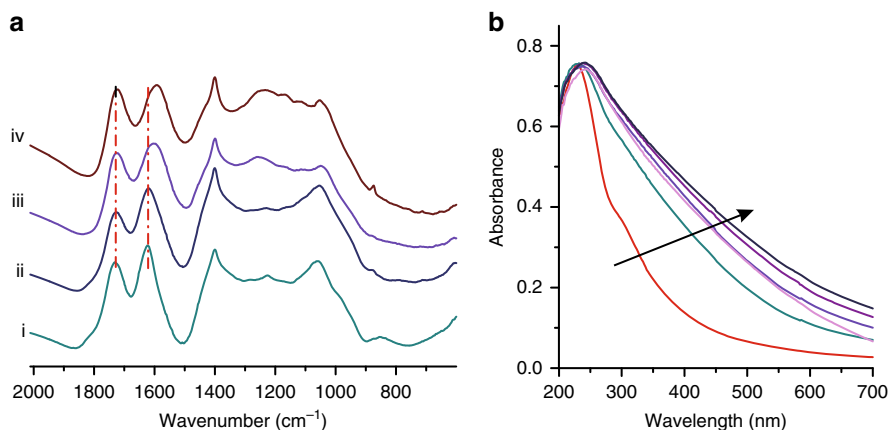
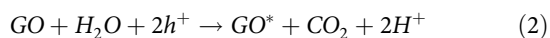


**Fig. 6** Spectroscopic analysis of GO particles during UV illumination. **a** FTIR of GO samples exposed to UV at different time: (i) pristine GO; (ii) 10 min; (iii) 60 min; (iv) 120 min. **b** UV-vis. absorption of GO samples exposed to UV at different time: 0, 5, 15, 30, 45, 60 min along the arrow

in the band gap of the semiconducting domains. Under the conditions of this work with weak light exposure, the photoreactions of GO involve both reversible and irreversible processes. The apparent irreversible process is the slow reduction reaction, where the oxygen-containing groups of GO are eliminated and the aromatic  $sp^2$  domains are expanded. It is evidenced by a darker color of the GO dispersion and UV-visible absorption spectra with an increase of absorption in the 280–800 nm range after long time UV exposure (Fig. 6b). The corresponding Fourier-transform infrared spectroscopy (FTIR) analysis reveals more details (Fig. 6a). Both the band at  $1730\text{ cm}^{-1}$  owing to the vibration of the C=O bond in carboxylic acids and the band at  $1400\text{ cm}^{-1}$  owing to the symmetric vibrations of the C–O bond in the carboxylate anion are almost not changed, whereas the band at  $1620\text{ cm}^{-1}$  arising from the C=C bonds in the  $sp^2$  domains becomes wider and shifts to  $1590\text{ cm}^{-1}$  indicative of the expansion of the aromatic  $sp^2$  domains. In the range from  $1000$  and  $1320\text{ cm}^{-1}$  corresponding to different stretching vibration modes of C–O in the alcohol and epoxide groups, relative intensities have been changed, indicating that transformation from epoxide to alcohol groups or elimination of some alcohol groups may happen. Some C–O bonds in the epoxide (2.1 eV) and in the tertiary alcohol group bound to GO (0.7 eV) can be cleaved in the photoreactions<sup>32</sup>. If comparing the UV-visible absorption spectrum of the sample exposed to UV for 5 min with the FTIR of the sample of UV for 10 min, it is noticed that the UV-visible absorption spectrum is obviously more sensitive than FTIR in reflecting UV caused early changes, because UV-visible absorption spectrum can monitor the electron excitation in semiconducting domains.

The apparent reversible photochemical/physical processes are evidenced by the light switchable and reversible change in the pH value and ionic conductivity (Fig. 5f). Considering the reversible change in pH and the above infrared spectroscopy analysis results, we figure that our results are consistent with the interpretation based on the electron and hole model<sup>31</sup>. According to the electron ( $e^-$ ) and hole ( $h^+$ ) model, the following reactions may happen under light above the band gap,



where  $GO^*$  is the reacted or reduced GO. The reaction (2) and (3) are carried out in the epoxy or hydroxyl groups of GO nanosheets<sup>31</sup>. Though these reactions can interpret the light-induced reversible change in pH, however, we did not observe any bubbles during the illumination processes, possibly because the reaction degree was very low actually, as also revealed from UV-vis. and FTIR spectroscopic analysis. Recently, we found that acetone can stabilize GO from being reduced by UV irradiation<sup>33</sup>. When we added acetone in the aqueous suspension of GO particles, the light-actuated swarming of GO particles was significantly inhibited (Fig. 7a), which could further support that the photoreactions of GO in water generated the propulsion force.

So far we have provided evidence that the GO particle with negative surface charges can generate an unbalanced ionic distribution surrounding it in a light field. The unbalanced ionic distribution surrounding the GO particles can cause a propulsion to the GO particles via two possible mechanisms, i.e., ionic diffusiophoresis or electrophoresis<sup>34</sup>. Diffusiophoresis of charged particles is driven by the macroscopic concentration gradient of an electrolyte. Self-electrophoresis is driven by the local electric field generated from the unbalanced ionic distribution. The two mechanisms are very confusing in many cases, because that the concentration gradient of an electrolyte in the ionic diffusiophoresis can also generate an electric field. However, the propulsion velocity in ionic diffusiophoresis is inversely proportional to the ionic concentration, thus is a hampered locomotion in salt-rich media<sup>35</sup>, which is a reliable method to distinguish ionic diffusiophoresis from electrophoresis. We investigated the effects of the addition of NaCl in a wide concentration range on the light-induced locomotion of GO particles. The results are plotted in Fig. 7b as the RMS velocity vs. the reciprocal of the molar concentration of NaCl added. In a broad range of NaCl concentration from  $0.01$  to  $10\text{ mmol L}^{-1}$ , the RMS velocity of GO particles increases a little with the addition of NaCl. When the concentration of NaCl reached  $1\text{ mol L}^{-1}$ , the GO particles were almost totally precipitated and not suitable for the investigation of self-propulsion. Electrophoresis has much higher tolerance to salts than ionic diffusiophoresis. The addition of NaCl at low concentrations could increase the amounts of ions attached on the surface of colloidal GO particles and the electrical conductivity, hence the electrophoresis velocity increased. Thus, the ionic diffusiophoresis mechanism can be ruled out. Overall, the self-propelled locomotion of the GO colloidal particles fits the profile of self-electrophoresis.

Based on the reactions (1–3), we figure out the self-electrophoresis mechanism of GO, as is depicted in Fig. 8. When



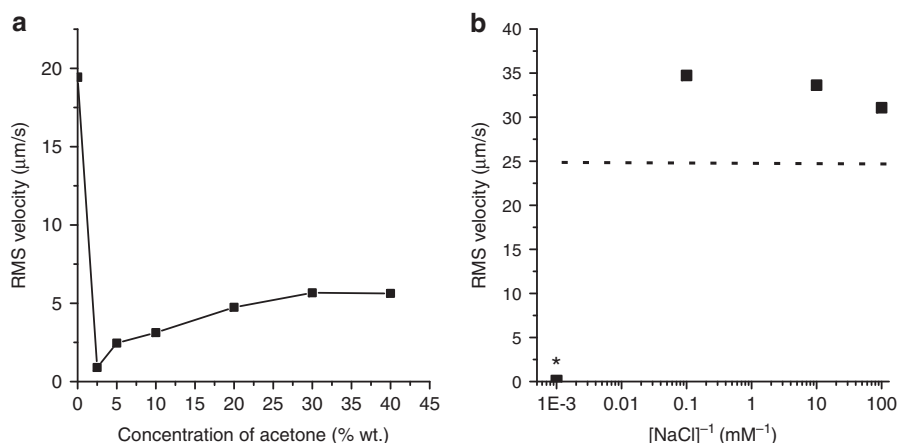


**Fig. 7** Effects of acetone and NaCl on the locomotion of GO particles. **a** Addition of acetone. **b** RMS velocity vs. the reciprocal of NaCl molar concentration. At the concentration of NaCl of 1 mol L<sup>-1</sup> marked with \*, the GO particles were precipitated and not suitable for the investigation of self-propulsion. The dashed line in **b** represents the RMS velocity without NaCl salt

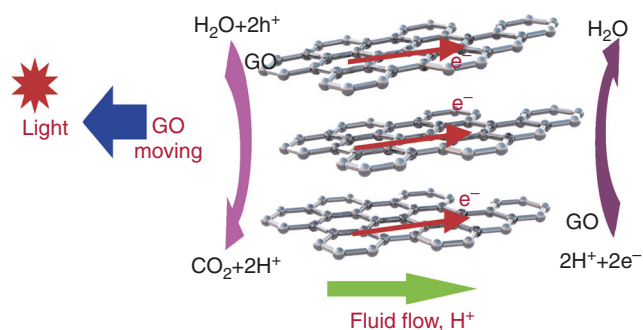


**Fig. 8** Schematic illustration of light-induced self-electrophoresis of a GO particle. Light above the threshold energy generates hydrogen ions in the bright side and a flux of electrons inside GO. The hydrogen ions flow from the bright side to the dark side along the particle surface. The GO particle moves towards the light source in the opposite direction to that of hydrogen ion flow

a GO particle is placed in a light field, the GO particle turns into an apparent Janus particle with both a dark side and a bright side, and the photoreactions start in the bright side where hydrogen ions are generated in the double electric layers of the GO particle and a flux of electrons inside GO. Thus, the GO particle generates its own hydrogen ion gradient around it, which presses hydrogen ion flow and electroosmotic fluid flow from the bright side to the dark side along the particle surface. The GO particle with a negative zeta potential moves towards the light source in the opposite direction to that of hydrogen ions and fluid flow, as actually observed.

Graphene is a zero band gap material. Our preliminary study found that graphene particles could also swarm to the center of light beam in pure water. But the swarming velocity of graphene particles was dependent on the surface stabilizer such as polyvinylpyrrolidone (PVP). If without surface stabilizer, graphene particles swarmed slowly with a RMS velocity of  $\sim 1 \mu\text{m s}^{-1}$  in a wide range of graphene contents from 0.1 to 0.5 mg mL<sup>-1</sup>. If stabilized with PVP, the graphene particles swarmed as fast as  $\sim 20 \mu\text{m s}^{-1}$  in 0.25 mg mL<sup>-1</sup> of graphene, indicating the light-induced locomotion of graphene particles may depend on the interfacial properties of graphene in water. Because of polar groups, GO particles do not need stabilizers for dispersing in water. Graphene defect structure for example around the holey

structure is possibly semiconducting. In addition, the absorbed light can excite graphene electrons extremely fast with a very high efficiency<sup>36</sup>, which may facilitate splitting water to generate ionic gradients. However, the self-driven motion of graphene needs further investigation in the future.

## Discussion

The unusual oscillatory behavior makes these GO particles more like active matter, as active matter is commonly defined as a collection of active particles, which are self-driven and exhibit a variety of non-equilibrium activities usually connected to motility<sup>37</sup>. Though we have provided evidence for the self-electrophoresis of these GO particles, however, it is puzzling why these GO particles undergo oscillatory motion. We want to discuss the possible oscillating mechanism in the following.

At first, we want to rule out some factors including turbulence in the solution from heating of GO aggregates or from fluid buoyancy due to possible CO<sub>2</sub> generated in the possible photochemical reactions of GO (e.g., equation 2), which if any could affect the dispersed GO particles more significantly than the fixed multilayer GO particles. However, the dispersed GO particles did not oscillate. Heat could enhance random thermal motion and disturb the transition from disorder to order phase in Vicsek model describing the collective behaviors of motile particles, but is unlikely to affect the propulsion in this work<sup>38</sup>.

Generally, two kinds of mechanisms could account for the oscillating behaviors of stacked GO particles, i.e., chemical oscillators or density fluctuation in collective motion.

It is well known that chemical oscillators exhibit nonlinear chemical dynamics<sup>26,39</sup>. Though we have related the breathing behavior to the stacked multilayer structures, however, we could not find substantial differences in any light-induced effects in above mentioned experiments between the dispersed GO and the stacked GO particles. Perhaps the change within the multilayer structures might account for the breathing phenomenon, for example, transition of electrons between stacked layers. The stacked multilayer structures of GO particles may be regarded as capacitors capable of periodic charging and discharging. The discharging process may change the surface charge density and hence the electric double layers over GO particles<sup>40,41</sup>, which is important for generating the interfacial force for driving colloidal particle<sup>4</sup>. But according to Fig. 5d, the zeta potential of the group of GO particles did not oscillate. Unfortunately, we cannot measure the zeta potential of an individual GO particle.

The oscillating frequency is very low, indicating that the collective motion is probably due to hydrodynamic interactions within these colloidal particles<sup>42,43</sup>.

The unusual oscillatory behavior is a possible consequence of collective behaviors. The collective behaviors of self-propelled particles are very complicated, which may cause motility-induced phase separation at very large particle density<sup>11,38</sup>, or flocking at finite contents<sup>44</sup>. If the randomly propelled particles autonomously follow the average velocity, 2D vortex with a void core can also be formed according to Herbert Levine et al.'s<sup>44</sup> work. Our observation in this work showed that light-actuated mobile GO particles flocked which was in accordance with Herbert Levine et al.'s<sup>44</sup> work obviously. However, we did not observe the 2D circular vortex on the horizontal plane possibly because that the direction of motile GO particles was not random actually. The flock in the core kept increasing when the light beam stimulus was switched on, and was finally visible to the naked eyes. There was no evidence that the flock in the core was eroded by vortex during swarming. But temporary localized vortex along GO moving direction was still possible, because we often observed the self-acceleration phenomena in this work or in our previous work<sup>14</sup>.

So far, no hydrodynamic model described the collective oscillating behavior of swarming colloidal particles. More attention is concentrated on the phase transition from disorder to order or the formation of pattern. However, it is commonly regarded that the movement speed of active particles decreases for density<sup>42</sup>. Thus, the density fluctuation is usually corresponding to velocity fluctuation. The oscillatory behavior of GO particles might be also a consequence of collective behaviors, though the oscillatory behavior is seldom observed.

Overall, we consider that the collective behavior could possibly account for the oscillation of stacked GO particles. In other words, the collective motion can perhaps cause cooperative motion apart from the emergence of orientational order. For example, flagella or cilia of bacteria function as a group to produce locomotion via harmonious motion<sup>45</sup>.

## Methods

**Synthesis of stacked multilayer GO particles fixed with hydrazine.** GO flake sample in pure water (18.3 M $\Omega$  cm) of 4 mL (2 mg mL<sup>-1</sup>) was ultrasonicated for 3 h, then centrifuged (1000 r min<sup>-1</sup>) for 2 minutes. The stable aqueous GO dispersion was collected and was vacuum-dried on a PTFE (Teflon) plate at 30 °C overnight to form a GO film with a diameter of 1.5 cm. The GO film was mixed with hydrazine (85% wt.) aqueous solution (0.5% v/v) of 1 mL for 30 min at room temperature. The N<sub>2</sub>H<sub>4</sub> fixed GO was filtered and repeatedly washed with pure water and ethanol, and then vacuum-dried at 30 °C for 3 h. The dry sample of N<sub>2</sub>H<sub>4</sub> fixed GO was dispersed in ultrapure water under ultrasonication for 3 h, and let it stand for 30 minutes to remove precipitated particles.

**Synthesis of stacked multilayer GO particles fixed with diamine.** GO in water (4 mg mL<sup>-1</sup>) was ultrasonicated for 3 h, then centrifuged (1000 r min<sup>-1</sup>) for 2 minutes. The stable aqueous GO dispersion was collected and was mixed with ethylene diamine or hexamethylene diamine aqueous solution (0.5% wt.) of 1 mL for 5 h. Then the chemically fixed GO particles were obtained by centrifugation at 8000 r min<sup>-1</sup> for 10 min, repeatedly washed with deionized water and ethanol, vacuum-dried at 30 °C for 3 h. Then the GO particles were dispersed in ultrapure water under ultrasonication for 3 h, and let them stand for 30 minutes to remove precipitated particles.

**Observation of the phototaxis of GO particles.** In total, 1 mL of GO aqueous suspension was placed in a 35 mm  $\times$  10 mm polystyrene petri dish for observing the light-induced kinematic behaviors of GO colloidal particles under an Olympus IX-81 inverted fluorescence microscope with its built-in illumination source (a 100 W mercury arc lamp) used as the light stimulus, as described in our previous work<sup>14</sup>. The light spot on the focal plane has a diameter of  $\sim$  2 mm. A  $\times$  20 objective was used for observing the particle motion and for focusing the light. The UV intensity of Olympus IX-81 can be attenuated from the strongest level 5 (UV energy densities 192 mW cm<sup>-2</sup>) to level 4 (89 mW cm<sup>-2</sup>), level 3 (34 mW cm<sup>-2</sup>) or weaker. The actual UV energy densities behind the polystyrene petri dish for level 5, level 4, and level 3 are measured to be 37 mW cm<sup>-2</sup>, 21 mW cm<sup>-2</sup>, and

11 mW cm<sup>-2</sup>, respectively, by using a standard UV energy meter. Real-time videos were taken by a CCD camera and recorded on a computer. By analyzing each separate frame of the video images, the displacement ( $\Delta L$ ) of a distinguishable GO particle at a certain time interval ( $\Delta t$ ) was measured. The mean square displacements  $\langle \Delta L^2 \rangle$  in two dimensions were obtained by averaging  $\sim$  30 GO particles. RMS velocity is calculated by  $\langle \Delta L^2 \rangle^{1/2} \Delta t^{-1}$ . The error bar is calculated as half of the standard deviation of  $\langle \Delta L^2 \rangle$ .

**Instruments.** FTIR analysis was carried out with Fourier Transform Infrared Spectrometer Nicolet 6700 (USA). XRD was performed with Multi-function target X-ray diffractometer (smartlab, Japan). Zeta potential was measured in NanoBrook 90Plus PALS (Brookhaven, USA).

AFM was performed on a DI Innova Scanning Probe Microscope (Veeco, USA) for imaging GO particles with special emphasis on sheet thickness and lateral dimensions. A few drops of the aqueous dispersion of GO (0.05 mg mL<sup>-1</sup>) were deposited on mica slice, and then vacuum-dried at 40 °C for 12 h. We measured the thickness and the longest dimension (Lateral size) of  $\sim$  100 objects observed in AFM as histograms.

## Data Availability

All relevant data are available from the authors upon reasonable request.

Received: 5 June 2018 Accepted: 8 October 2018

Published online: 26 October 2018

## References

- Ismagilov, R. F., Schwartz, A., Bowden, N. & Whitesides, G. M. Autonomous movement and self-assembly. *Angew. Chem. Int. Ed.* **41**, 652–654 (2002).
- Paxton, W. F., Sundararajan, S., Mallouk, T. E. & Sen, A. Chemical locomotion. *Angew. Chem. Int. Ed.* **45**, 5420–5429 (2006).
- Sánchez, S., Soler, L. & Katuri, J. Chemically powered micro- and nanomotors. *Angew. Chem. Int. Ed.* **54**, 1414–1444 (2015).
- Anderson, J. L. Colloid transport by interfacial forces. *Annu. Rev. Fluid. Mech.* **21**, 61–99 (1989).
- Pedley, T. J. & Kessler, J. O. Hydrodynamic phenomena in suspensions of swimming microorganisms. *Annu. Rev. Fluid. Mech.* **24**, 313–358 (1992).
- Kagan, D. et al. Chemical sensing based on catalytic nanomotors: motion-based detection of trace silver. *J. Am. Chem. Soc.* **131**, 12082–12083 (2009).
- Jimmy, F. & Pilar, R. M., & E, R. D. Phase-selective catalysis in emulsions stabilized by janus silica-nanoparticles. *Adv. Synth. Catal.* **352**, 2359–2364 (2010).
- Sheng, M. J. G. & Martin, P. Chemical energy powered nano/micro/macro motors and the environment. *Chem. A Eur. J.* **21**, 58–72 (2015).
- Mou, F. et al. Autonomous motion and temperature-controlled drug delivery of Mg/Pt-Poly(N-isopropylacrylamide) Janus micromotors driven by simulated body fluid and blood plasma. *ACS Appl. Mater. Interfaces* **6**, 9897–9903 (2014).
- Fusco, S. et al. Shape-switching microrobots for medical applications: the influence of shape in drug delivery and locomotion. *ACS Appl. Mater. Interfaces* **7**, 6803–6811 (2015).
- Narayan, V., Ramaswamy, S. & Menon, N. Long-lived giant number fluctuations in a swarming granular nematic. *Science* **317**, 105–108 (2007).
- Bricard, A., Caussin, J.-B., Desreumaux, N., Dauchot, O. & Bartolo, D. Emergence of macroscopic directed motion in populations of motile colloids. *Nature* **503**, 95–98 (2013).
- Palacci, J., Sacanna, S., Steinberg, A. P., Pine, D. J. & Chaikin, P. M. Living crystals of light-activated colloidal surfers. *Science* **339**, 936–940 (2013).
- Li, W., Wu, X., Qin, H., Zhao, Z. & Liu, H. Light-driven and light-guided microswimmers. *Adv. Funct. Mater.* **26**, 3164–3171 (2016).
- Mehes, E. & Vicsek, T. Collective motion of cells: from experiments to models. *Integr. Biol.* **6**, 831–854 (2014).
- Kotar, J., Leoni, M., Bassetti, B., Lagomarsino, M. C. & Cicuta, P. Hydrodynamic synchronization of colloidal oscillators. *Proc. Natl. Acad. Sci.* **107**, 7669–7673 (2010).
- András, C., Stanley, H. E. & Tamás, V. Spontaneously ordered motion of self-propelled particles. *J. Phys. A. Math. Gen.* **30**, 1375–1385 (1997).
- Bozorgi, Y. & Underhill, P. T. Effects of elasticity on the nonlinear collective dynamics of self-propelled particles. *J. Non-Newton. Fluid Mech.* **214**, 69–77 (2014).
- Kim, J., Cote, L. J. & Huang, J. Two dimensional soft material: new faces of graphene oxide. *Acc. Chem. Res.* **45**, 1356–1364 (2012).
- Novoselov, K. S. et al. Electric field effect in atomically thin carbon films. *Science* **306**, 666–669 (2004).

21. Chen, X., Wu, G., Lan, T. & Chen, W. Autonomous micromotor based on catalytically pneumatic behavior of balloon-like MnOx-graphene crumples. *Chem. Commun.* **50**, 7157–7159 (2014).
22. Qin, C. et al. Laser-driven propulsion of multilayer graphene oxide flakes. *J. Mater. Chem. C* **6**, 2329–2335 (2018).
23. Ma, X., Katuri, J., Zeng, Y., Zhao, Y. & Sanchez, S. Surface conductive graphene-wrapped micromotors exhibiting enhanced motion. *Small* **11**, 5023–5027 (2015).
24. McAllister, M. J. et al. Single sheet functionalized graphene by oxidation and thermal expansion of graphite. *Chem. Mater.* **19**, 4396–4404 (2007).
25. Varrla, E. et al. Large-scale production of size-controlled MoS<sub>2</sub> nanosheets by shear exfoliation. *Chem. Mater.* **27**, 1129–1139 (2015).
26. Altemose, A. et al. Chemically controlled spatiotemporal oscillations of colloidal assemblies. *Angew. Chem. Int. Ed.* **56**, 7817–7821 (2017).
27. Paxton, W. F., Sen, A. & Mallouk, T. E. Motility of catalytic nanoparticles through self-generated forces. *Chem. A Eur. J.* **11**, 6462–6470 (2005).
28. Paxton, W. F. et al. Catalytically induced electrokinetics for motors and micropumps. *J. Am. Chem. Soc.* **128**, 14881–14888 (2006).
29. Qi, X. et al. Ultraviolet, visible, and near infrared photoresponse properties of solution processed graphene oxide. *Appl. Surf. Sci.* **266**, 332–336 (2013).
30. Gengler, R. Y. N. et al. Revealing the ultrafast process behind the photoreduction of graphene oxide. *Nat. Commun.* **4**, 2560–2565 (2013).
31. Matsumoto, Y. et al. Photoreaction of graphene oxide nanosheets in water. *J. Phys. Chem. C* **115**, 19280–19286 (2011).
32. Stroyuk, A. L. et al. Photochemical reduction of graphene oxide in colloidal solution. *Theor. Exp. Chem.* **48**, 2–13 (2012).
33. Qin, H., Zhu, Q. & Liu, H. Stabilization of Aqueous Graphene Oxide with Acetone under gamma-Ray/UV Irradiation. *Chinese J. Chem. Phys.* **31**, in press, <https://doi.org/10.1063/1674-0068/31/cjcp1803048> (2018).
34. Prieve, D. C., Anderson, J. L., Ebel, J. P. & Lowell, M. E. Motion of a particle generated by chemical gradients. Part 2. Electrolytes. *J. Fluid. Mech.* **148**, 247–269 (1984).
35. Ibele, M., Mallouk Thomas, E. & Sen, A. Schooling behavior of light-powered autonomous micromotors in water. *Angew. Chem. Int. Ed.* **48**, 3308–3312 (2009).
36. Tomadin, A. et al. The ultrafast dynamics and conductivity of photoexcited graphene at different Fermi energies. *Sci. Adv.* **4**, eaar5313 (2018).
37. De Magistris, G. & Marenduzzo, D. An introduction to the physics of active matter. *Phys. A: Stat. Mech. its Appl.* **418**, 65–77 (2015).
38. Vicsek, T. & Zafeiris, A. Collective motion. *Phys. Rep.* **517**, 71–140 (2012).
39. Epstein, I. R. & Showalter, K. Nonlinear chemical dynamics: oscillations, patterns, and chaos. *J. Phys. Chem.* **100**, 13132–13147 (1996).
40. Partenskii, M. B. & Jordan, P. C. “Squishy capacitor” model for electrical double layers and the stability of charged interfaces. *Phys. Rev. E* **80**, 011112 (2009).
41. Partenskii, M. B. & Jordan, P. C. Relaxing gap capacitor models of electrified interfaces. *Am. J. Phys.* **79**, 103–110 (2011).
42. Beatus, T., Tlusty, T. & Bar-Ziv, R. Phonons in a one-dimensional microfluidic crystal. *Nat. Phys.* **2**, 743–748 (2006).
43. Gomilšek, M. et al. Light-driven oscillations of entangled nematic colloidal chains. *Eur. Phys. J. E* **33**, 291–296 (2010).
44. Levine, H., Rappel, W.-J. & Cohen, I. Self-organization in systems of self-propelled particles. *Phys. Rev. E* **63**, 017101–017104 (2000).
45. Jahn, T. L. & Bovee, E. C. Movement and locomotion of microorganisms. *Annu. Rev. Microbiol.* **19**, 21–58 (1965).

### Acknowledgements

Financial support from the National Science Foundation of China (21274135 and 51673181).

### Author contributions

H.Q. performed the experiments. H.Q. and H.L. analyzed the data. X.W. and X.X. developed some experimental methods. H.L. conceived and directed the research. All authors contributed to the manuscript.

### Additional information

Supplementary information accompanies this paper at <https://doi.org/10.1038/s42004-018-0073-4>.

**Competing interests:** The authors declare no competing interests.

**Reprints and permission** information is available online at <http://npg.nature.com/reprintsandpermissions/>

**Publisher's note:** Springer Nature remains neutral with regard to jurisdictional claims in published maps and institutional affiliations.



**Open Access** This article is licensed under a Creative Commons Attribution 4.0 International License, which permits use, sharing, adaptation, distribution and reproduction in any medium or format, as long as you give appropriate credit to the original author(s) and the source, provide a link to the Creative Commons license, and indicate if changes were made. The images or other third party material in this article are included in the article's Creative Commons license, unless indicated otherwise in a credit line to the material. If material is not included in the article's Creative Commons license and your intended use is not permitted by statutory regulation or exceeds the permitted use, you will need to obtain permission directly from the copyright holder. To view a copy of this license, visit <http://creativecommons.org/licenses/by/4.0/>.

© The Author(s) 2018